Chemical Engineering Journal 371 (2019) 461–469

Contents lists available at ScienceDirect

Chemical Engineering Journal

journal homepage: www.elsevier.com/locate/cej

MOF derived Ni-Co-S nanosheets on electrochemically activated carbon cloth via an etching/ion exchange method for wearable hybrid supercapacitors

Wei Zhao[a,b,1], Yiwei Zheng[a,b,1], Liang Cui[a,*], Dedong Jia[b], Di Wei[a], Rongkun Zheng[a], Colin Barrow[c], Wenrong Yang[c], Jingquan Liu[a,b,*]

[a] College of Materials Science and Engineering, Linyi University, Linyi 276400, Shandong, China
[b] College of Materials Science and Engineering, Institute for Graphene Applied Technology Innovation, Qingdao University, Qingdao 266071, Shandong, China
[c] Biodeakin, School of Life and Environmental Sciences, Deakin University, Victoria 3217, Australia

HIGHLIGHTS

- MOFs were utilized as templates to obtain porous nanostructure.
- Electrochemical activation endowed CC with excellent hydrophilic property.
- Unique hydrolysis and ion exchange/etching method was used in this work.
- The hybrid supercapacitor exhibited excellent flexibility and wearability.

ARTICLE INFO

Keywords:
Electrochemically activated carbon cloth
MOF
Etching/ion exchange
Flexible and wearable supercapacitors

ABSTRACT

Flexible electrodes with favorable architectures are urgently demanded for flexible and wearable supercapacitors with high performance. Herein, we demonstrate the rational design and preparation of hollow and ultrathin nickel cobalt sulfides nanosheets arrays on electrochemical activated carbon cloth (Ni-Co-S/ACC) for fabrication of flexible hybrid supercapacitors, where the Ni-Co-S nanosheets are derived from the metal-organic framework via an etching/ion exchange method. The Ni-Co-S/ACC electrode can deliver a very high specific capacitance of 2392 F/g at the current density of 1 A/g and good rate performance (80.3% capacitance retention at 20 A/g). The enhanced electrochemical properties should be attributed to the hydrophilic property, good conductivity and enriched redox active sites resulted from the electrochemical activated carbon cloth and the hollow and ultrathin structure of Ni-Co-S nanosheets. When a flexible hybrid supercapacitor is assembled using Ni-Co-S/ACC as positive electrode and activated carbon as negative electrode, it shows high energy density of 30.1 Wh/Kg at power density of 800.2 W/Kg as well as predominant cycling stability (82% retention after 10,000 cycles). Furthermore, the excellent flexibility and wearability of the hybrid supercapacitor could envision promising applications in high-performance wearable energy storage devices.

1. Introduction

To meet the growing requirement of energy sources, great efforts have been devoted to develop high-power energy storage devices and energy conversion equipments. Supercapacitors (SCs) have attracted widespread attentions due to their remarkable properties such as quick-acting charging-discharging time (high power density) and good cycling life [1–3]. Moreover, owning to the increasing demands for portable and wearable electronic devices such as collapsible screens, flexible supercapacitors have been extensively explored [4,5]. However, compared with rechargeable batteries, SCs have shown lower capacity or energy density due to their charge storage mechanism only occurs on the surface or near surface of electrode materials. As a result, much more concern has been focused to improve their energy density.

It is well known that the energy density of SCs is mainly related to the specific capacitance (C) and operating voltage window (V),

* Corresponding authors at: College of Materials Science and Engineering, Linyi University, Linyi 276400, Shandong, China (J. Liu).
E-mail addresses: cuiliang@lyu.edu.cn (L. Cui), jliu@qdu.edu.cn (J. Liu).
[1] These authors contributed equally to this work.

https://doi.org/10.1016/j.cej.2019.04.070
Received 21 January 2019; Received in revised form 20 March 2019; Accepted 10 April 2019
Available online 11 April 2019
1385-8947/

therefore, many efforts have been devoted to obtain the SCs with high energy density through exploring the porous, nano-sized capacitive and pseudocapacitive electrode materials, and/or developing asymmetric and hybrid SCs for wide operating voltage window [6]. Transition metal oxides and hydroxides such as Co_3O_4 and $Ni(OH)_2$ exhibit superior capacitance due to their rich redox reaction for charge storage [7–11]. Nevertheless, these materials usually display poor conductivity and unpleasant electrochemical stability which severely hinder their practical applications. Recently, transition metal sulfides, especially ternary sulfides, have been widely explored as high electrochemical performance SCs. The substitution of sulfur for oxygen results in the formation of the more flexible structures own to the lower electronegativity of sulfur than oxygen, leading to the less collapse and more stability of structure. Furthermore, ternary transition metal sulfides display much lower optical band gaps and much higher conductivity than binary sulfides, which could result in excellent rate performance [12]. For example, the electrical conductivity of $NiCo_2S_4$ is about 100 times higher than that of $NiCo_2O_4$ and four orders of magnitude higher than that of nickel or cobalt oxides because of its smaller band gap [13,14].

In addition to seeking high-performance materials as electrodes, rational design of the structure of electrode materials can also be an efficient alternative to enhance the electrochemical kinetics [15]. Metal-organic framework (MOF), a kind of advanced materials with metal centers and organic blocks, has been considered to be very promising for gas adsorption, supercapacitor and catalysis due to their well-ordered structure, large surface area, high porosity and diverse topology, all of which endow MOF with tunable functionalities for wide applications [16–18]. Especially, taking advantage of its high specific surface area and porosities, MOFs have consequently been utilized as template to prepare porous nanostructure with high surface area for high-capacitance SCs owning to the fact that they can shorten the diffusion length and offer more active sites.

Herein, we demonstrate, for the first time, the fabrication of MOF derived ultrathin and porous $NiCo_2S_4$ nanosheets arrays with enriched edge sites on electrochemically-activated flexible carbon cloth (ACC) and the application as positive electrode for high-performance flexible ASCs. The electrochemically treated carbon cloth substrate exhibits excellent flexibility and hydrophilic property. The rational design of MOF makes it possible to obtain $NiCo_2S_4$ nanosheets arrays with increased structural robustness. Upon the unique hydrolysis and etching process in the presence of $Ni(NO_3)_2$ and Na_2S, the obtained $NiCo_2S_4$ arrays exhibit ultrathin and porous nanosheet structures, which provide high specific surface area and rich active sites to facilitate electrolyte penetration and shorten the ion diffusion path, therefore are beneficial for the improvement of electrochemical performance. As a result, the prepared active electrode materials exhibit a high specific capacitance of 2392 F/g at 1 A/g and excellent rate capability of 80.3% at 20 A/g. The assembled hybrid supercapacitor delivers a high energy density of 30.1 Wh/Kg at a power density of 800.2 W/Kg and excellent cycling stability. Great potential of $NiCo_2S_4$/ACC electrode for assembling the flexible wearable supercapacitors can be demonstrated by lighting up the red LED and charging a watch when it is utilized for fabrication of a wristband supercapacitor.

2. Experiment section

2.1. Synthesis of electrochemical activated carbon cloth

Firstly, a piece of commercial carbon cloth (1 cm × 2.5 cm) was cleaned with absolute ethanol, acetone and ultrapure water in sequence. Electrochemical activation of the above cleaned carbon cloth was realized by utilizing a three-electrode configuration in a mixed solution of HNO_3 and H_2SO_4 (volume ratio = 1) with a constant voltage of 3 V for 180 s. In this system, a platinum plate was used as counter electrode and saturated calomel electrode (SCE) as reference electrode. Then the resulted activated carbon cloth (ACC) was washed with ultrapure water and dried in vacuum at 60 °C.

2.2. Synthesis of Ni-Co precursor/ACC

Firstly, 1.3136 g of 2-methylimidazole ($C_4H_6N_2$) was added into 40 mL ultrapure water under magnetic stirring to afford a uniform dispersion. Then 0.5821 g of $Co(NO_3)_2{\cdot}6H_2O$ was dispersed into 40 mL ultrapure water by stirring for 3 min. The $C_4H_6N_2$ aqueous solution was poured into $Co(NO_3)_2{\cdot}6H_2O$ dispersion quickly, followed by the addition of a piece of ACC. After the reaction for 4 h, the prepared sample was taken out, washed with ultrapure water and dried in vacuum at 60 °C for 12 h. Subsequently, the obtained product was dipped into the $Ni(NO_3)_2{\cdot}6H_2O$ solution (0.01 M, 100 mL) in ethanol for 15 min under magnetic stirring. Finally, the expected product of Ni-Co precursor/ACC was taken out, cleaned with absolute ethanol and dried at 60 °C in a vacuum drying oven.

2.3. Synthesis of $NiCo_2S_4$/ACC

In a typical procedure, 0.68 g of $Na_2S{\cdot}9H_2O$ was dissolved in 40 mL ultrapure water under constant magnetic stirring to obtain a uniformly dispersed solution. Then the above aqueous solution together with the Ni-Co precursor/ACC was transferred into a 50 mL Taflon-lined stainless steel autoclave. The hydrothermal reaction was conducted at 160 °C for 8 h. After cooling down naturally to room temperature, the resulting product (abbreviated as Ni-Co-S/ACC-160) was collected, washed with ultrapure water and dried at 60 °C overnight. By contrast, $NiCo_2S_4$ on untreated carbon cloth ($NiCo_2S_4$/CC) was also synthesized under the same condition. In order to explore the optimum curing temperature, the sulfuration of Ni-Co precursor was also performed at 120 °C and 200 °C to afford the products which are abbreviated as Ni-Co-S/ACC-120 and Ni-Co-S/ACC-200, respectively.

2.4. Preparation of flexible hybrid supercapacitors device

To assemble a flexible hybrid supercapacitor, the as-prepared Ni-Co-S/ACC was utilized as positive electrode. Activated carbon, acetylene black and polyvinylidene fluoride (PVDF) were mixed homogeneously with a mass ratio of 85:10:5 and deposited on the surface of a piece of ACC (1 × 2.5 cm^2). The PVA-KOH gel electrolyte was prepared by mixing 6 M KOH solution and 2.5 g PVA in 20 mL ultrapure water at 90 °C under stirring until the solution became clear. The PVA-KOH gel electrolyte was sandwiched between Ni-Co-S/ACC positive electrode and negative electrode.

2.5. Material characterizations

Field emission scanning electron microscopy (FE-SEM, FEI Quanta200F) and transmission electron microscopy (TEM, JEM-1200 EX) were utilized to analyze the morphology and structure of the prepared materials. X-ray diffraction (XRD, D8-Advance, Bruker) was used to characterize the crystal structure and X-ray photoelectron spectroscopy (XPS) was carried out on a Kratos AXIS Ultra DLD spectrometer to characterize the chemical state and the surface-bound functionalities of $NiCo_2S_4$/ACC.

2.6. Electrochemical measurement

The electrochemical properties of prepared electrode materials were evaluated by an electrochemical station (CHI 660D) with a standard three-electrode system in 6 M KOH aqueous solution wherein Pt and Hg/HgO electrode were used as counter and reference electrode, respectively. The electrochemical properties were investigated via cyclic voltammetry (CV) with the increasing scan rate from 5 to 50 mV/s, galvanostatic charge/discharge (GCD) with different current densities

varying from1 to 20 A/g and electrochemical impedance spectrometry (EIS) in frequency ranging from 100 kHz to 0.01 Hz.

The specific capacitances were calculated via the following equation:

$$C_M = \frac{I\Delta t}{m\Delta V} \quad (1)$$

where C_M denotes the specific mass capacitance (F/g), I is discharge current (A), Δt indicates the discharge time (s), m refers to the mass of active materials (g) and ΔV represents the operated potential window (V).

The assembled hybrid supercapacitor was evaluated via a two-electrode system. The power density (P, W/Kg) and energy density (E, Wh/Kg) were calculated based on the total mass of active material on positive and negative electrodes by the following equations:[19,20]

$$E = \frac{1}{2}C_M\Delta V^2 \quad (2)$$

$$P = \frac{E}{\Delta t} \quad (3)$$

3. Results and discussion

3.1. Material fabrication and characterizations

The stepwise fabrication process of MOF derived porous $NiCo_2S_4$ on electrochemical-activated flexible carbon cloth (ACC) is depicted in Fig. 1a. The flexible ACC substrate was obtained by activating the commercial carbon cloth via an electrochemical method (details can be seen in Experimental section) and then was submerged in the mixture of 2-methylimidazole ($C_4H_6N_2$) and $Co(NO_3)_2{\cdot}6H_2O$ aqueous solution for 4 h to obtain the cobalt based MOF solid nanoarrays covered ACC (abbreviated as Co-MOF/ACC). In this step, electrochemical activation introduced a large amount of oxygenous groups, thus endowed carbon cloth with excellent hydrophilic property, which facilitated the uniform growth of Co-MOF on the surface of carbon fiber. $Ni(NO_3)_2$ was utilized subsequently to etch Co-MOF via an ion exchange process for the preparation of ultrathin Ni-Co layered double hydroxide (Ni-Co LDH/ACC), whose formation mechanism could be speculated as following: $Ni^{2+} + 2H_2O \rightarrow Ni(OH)_2 + 2H^+$, where Ni^{2+} is hydrolyzed to yield $Ni(OH)_2$ and H^+. The H^+ ions could etch the MOF and make for the deposition of Ni-Co LDH simultaneously [21]. Finally, Ni-Co LDH/ACC was converted to $NiCo_2S_4$/ACC by hydrothermal sulfuration reaction with Na_2S as the sulfur source. S^{2-} in the system could also act as etching agent, leading to the formation of ultrathin edge site-enriched $NiCo_2S_4$ nanoarrays on ACC ($NiCo_2S_4$/ACC) [22].

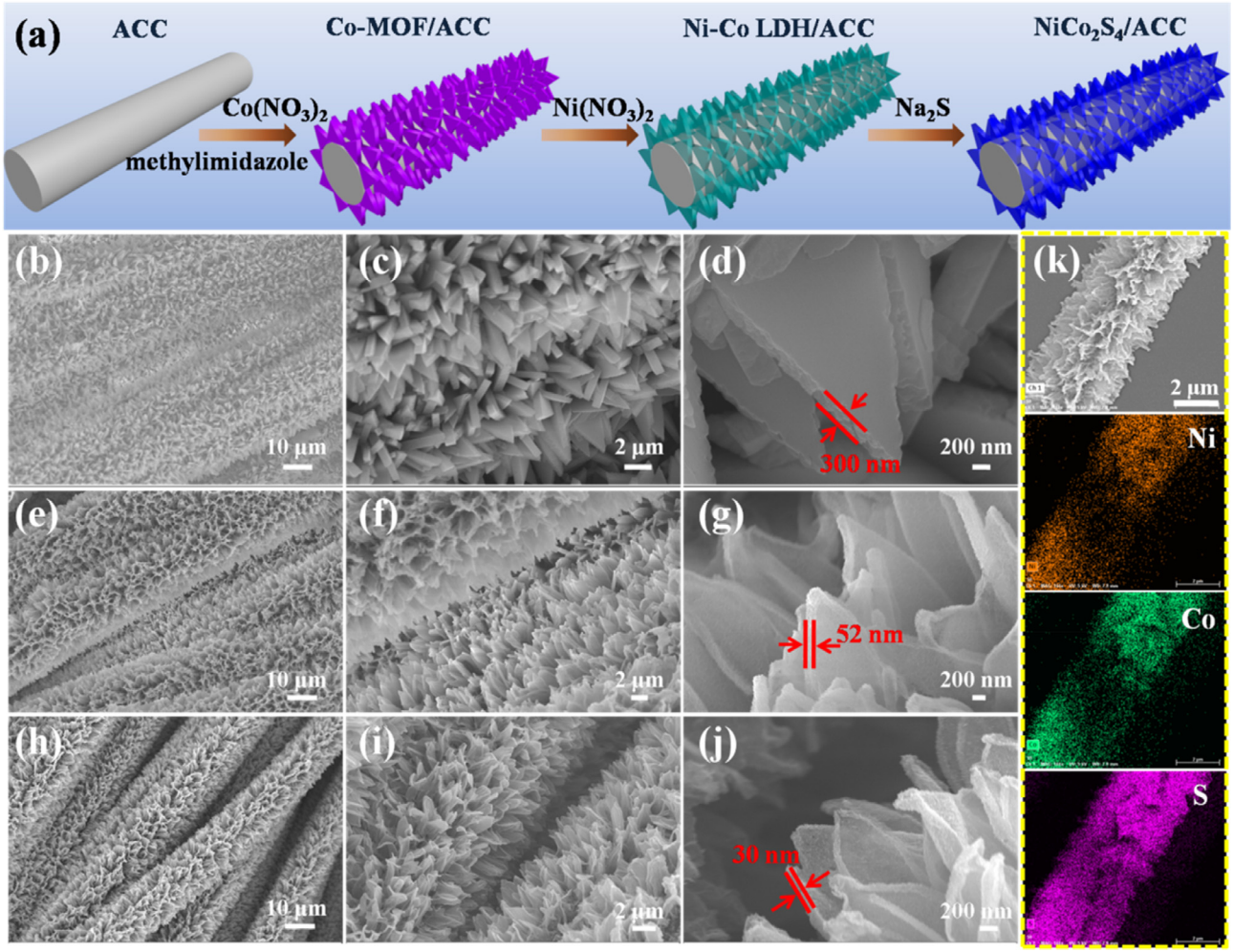

Fig. 1. (a) Schematic illustration for the synthesis of MOF derived ultrathin $NiCo_2S_4$ nanoarrays on electrochemical activated carbon cloth. (b) Low and (c, d) high magnification SEM images of Co-MOF/ACC. (e) Low and (f, g) high magnification SEM images of Ni-Co LDH/ACC. (h) Low and (i, j) high magnification SEM images of $NiCo_2S_4$/ACC-160. (k) SEM and the corresponding elemental mapping images of $NiCo_2S_4$/ACC-160.

It's well known that most carbon based materials exhibit inherent hydrophobic properties, which is disadvantageous for the growth of active materials when they are utilized as substrates. On the other hand, the hydrophobicity also impedes the penetration of electrolytes and therefore unavoidably encounters bottlenecks in improving their electrochemical performance for SCs [23]. In this work, the commercial carbon cloth was firstly activated via electrochemical oxidization in mixed acid solution (H_2SO_4–HNO_3) at a constant potential of 3 V for 180 s. After that, the oxygen functional groups were introduced on the surface of carbon fibers will enhance the wettability of substrate, making the feasible growth of Co-MOF on ACC [24]. The hydrophilic property was characterized by measuring the dynamic water contact angle. Fig. S1a shows that ACC has excellent wettability and a droplet of water can be absorbed immediately within one second. The scanning electron microscopy (SEM) image and the inset digital image (Fig. S1b) of Co-MOF/ACC indicate that the Co-MOF nanoarrays have uniformly grown on the whole fibers of ACC. In contrast, the contact angle of untreated CC (Fig. S2a) is 134° under the same testing condition, demonstrating the significant hydrophobicity. Correspondingly, the growth of Co-MOF on CC substrate displays severe agglomeration and unevenness on the surface of CC as evidenced by the SEM image and corresponding digital photo as shown in Fig. S2b, which should be due to the hydrophobic property that heavily hinders the access of Co $(NO_3)_2$ and $C_4H_6N_2$ onto the carbon fibers to form Co-MOF/CC.

SEM images of Co-MOF/ACC shown in Fig. 1b, c, demonstrate the uniform coverage of Co-MOF nanosheets arrays on the surface of ACC. The enlarged view in Fig. 1d displays the smooth surface of the solid nanosheets with the thinness of 300 nm. After reactions of the Co-MOF nanowalls with $Ni(NO_3)_2$ for 15 min, the monolithic nanoarrays have been maintained as shown in Fig. 1e, f. As can be seen in Fig. 1g, the thinness of nanowalls is about 52 nm, which is obviously thinner than those before reaction with $Ni(NO_3)_2$, indicating the successful etching process. The short-time (5 min) etching treatment using $Ni(NO_3)_2$ would result in insufficient etching and semi-hollow nanosheets, whereas too long-time (25 min) treatment would generate the excessive etching product with destructive structure as shown in Fig. S3.

The SEM images of Ni-Co-S/ACC-160 are presented in Fig. 1(h-j). The dense and uniform coverage of Ni-Co-S nanosheets on the surface of carbon fiber testified that the nanoarray structure could be retained intact after hydrothermal reaction at 160 °C for 8 h as shown in Fig. 1(h-i). Furthermore, the nanosheets with crimp edges became thinner(less than 30 nm) and even semitransparent, evidencing the formation of hollow structure after the etching process in the presence of $Ni(NO_3)_2$ and Na_2S. The ultrathin Ni-Co-S nanosheets with hollow and porous structure could effectively shorten the pathway of electrolyte ions diffusion and facilitate the insertion/disembedding process during the charge–discharge cycles [25]. As presented in Fig. 1k the elemental mapping images of Ni-Co-S/ACC-160 indicate the presence of Ni, Co and S.

The morphology of stepwise prepared samples was further investigated by transmission electron microscopy (TEM) analysis and the corresponding TEM images are displayed in Fig. 2. As revealed by the TEM images in Fig. 2a and b, the nanosheets of Co-MOF presents a solid characteristic, which are converted into thinner nanosheets with hollow structure after reacting with $Ni(NO_3)_2$ as shown in Fig. 2c. From the magnified TEM image (Fig. 2d), a mass of wrinkles can be observed, which is in coincidence with SEM results. After hydrothermal sulfuration treatment, the ultrathin nanosheets with well-maintained structure have been obtained with numerous nanoparticles distributed uniformly on the surface as manifested in Fig. 2e and f). High resolution TEM (HRTEM) image of Ni-Co-S/ACC-160 is presented in Fig. 2g, from which the crystal lattice of 0.17 nm, 0.24 nm and 0.28 nm are derived, which match perfectly with the 440, 400 and 311 planes of $NiCo_2S_4$ (JCPDF NO. 20-0782) [26]. The inserted selected area electron diffraction (SAED) as shown in Fig. 2g exhibits continuous diffraction rings, which indicate the presence of different crystal planes with polycrystalline feature on the nanosheets.

The crystal structure of obtained samples was further studied via X-ray diffraction (XRD). From the XRD results shown in Fig. 2h, the characteristic peaks of amorphous carbon can be clearly observed at 25.6° and 38.5° [27]. The diffraction peaks of the prepared Ni-Co-S/ACC-160 at 31.5°, 38.2°, 50.7° and 55.1° can be well indexed to (3 1 1), (4 0 0), (5 1 1) and (4 4 0) planes of $NiCo_2S_4$ cubic phase (JCPDF NO. 20–0782) respectively, indicating the successful transformation from NiCo-LDH (Fig. S4) to $NiCo_2S_4$.

The chemical state and composition of prepared Ni-Co-S/ACC-160 were further investigated by XPS. As shown in Fig. 3 the XPS survey spectrum of Ni-Co-S/ACC-160 (Fig. 3a) demonstrates the presence of Ni, Co, O, C and S elements without any other impurities. The elements C and O should come from ACC while Ni, Co and S are ascribed to the generation of $NiCo_2S_4$. The C 1s spectrum (Fig. 3b) can be fitted into four peaks corresponding to −COOH (288.5 eV), >C═O (287.2 eV), >COH (286.3 eV) and C−C (284.8 eV), confirming the successful introduction of functional groups on the surface of carbon fiber after electrochemical activation. The binding energies of O1s spectrum as shown in Fig. 3c can be deconvoluted into three different peaks at 533.18 eV, 532.31 eV and 531.63 eV, which are attributed to −COOH, >COH and >C═O, respectively.

In Fig. 3d, the spectrum of Ni 2p can be fitted well with two spin–orbit doublets and two shakeup satellites (abbreviated as Sat) by a Gaussian fitting method, evidencing the presence of of Ni^{2+} and Ni^{3+}. The peaks centered at 853.6 eV and 872.5 eV correspond to Ni^{2+}, while the peaks located at 856.4 eV and 874.5 eV are assigned to Ni^{3+} [28]. Two peaks observed in the spectrum of Co 2p (Fig. 3e) at 781.5 eV and 797.7 eV are characteristic of Co^{2+}. The binding energy values at 779.1 eV and 794.1 eV are typical peaks of Co^{3+}. For the S 2p spectrum as shown in Fig. 3f, two main peaks at 161.8 eV for $2p_{3/2}$ and 162.8 eV for $2p_{1/2}$ and one shakeup satellite at 169.1 eV are observed, where the peak at 161.8 eV is representative of metal-sulfur bonds while the peak at 162.8 eV should be ascribed to sulfur ions at low coordination ordinarily related to sulfur vacancies. According to the above discussed results, the near surface of prepared Ni-Co-S/ACC-160 has a mixed composition containing Ni^{2+}, Ni^{3+}, Co^{2+} and Co^{3+}, which is favorable for a supercapacitor to achieve high electrochemical performance by providing rich Faradic reaction sites.

3.2. Electrochemical performance

Electrochemical measurements of $NiCo_2S_4$/ACC were implemented in a three-electrode system with 6 M KOH solution as electrolyte. Fig. 4a exhibits the cyclic voltammetry (CV) curves of Ni-Co-S/ACC-120, Ni-Co-S/ACC-160 and Ni-Co-S/ACC-200 at a potential window between 0 and 0.55 V with the scan rate of 10 mV/s. Obviously, the CV area of Ni-Co-S/ACC-160 is larger than those of the other two electrode materials as prepared, demonstrating the optimal electrochemical capacitance can be obtained by selecting the proper hydrothermal temperature. Furthermore, the pair of oxidation/reduction peaks of Ni-Co-S/ACC-160 are more sharp and the potential difference (E_O-E_R) between the oxidation potential (E_O) and reduction potential (E_R) is smaller than those of the other two, indicating the better reaction reversibility and faster reaction kinetics process for the electrode material prepared at 160 °C [29]. The discharge time for Ni-Co-S/ACC-160 is longer than those for other samples as depicted in the galvanostatic charge discharge (GCD) curves (Fig. 4b), suggesting the highest capacitance.

The electrochemical impedance spectrometry (EIS) measurement was also performed to analyze the electrochemical behaviors of the three prepared electrode materials. Fig. 4c shows that the slopes of the straight lines for Ni-Co-S/ACC-160 and Ni-Co-S/ACC-200 are almost the same, which are significantly larger than that of Ni-Co-S/ACC-120 in the low-frequency region, revealing the lower diffusion resistance (Rw) and charge transfer resistance (Rct). Moreover, the equivalent

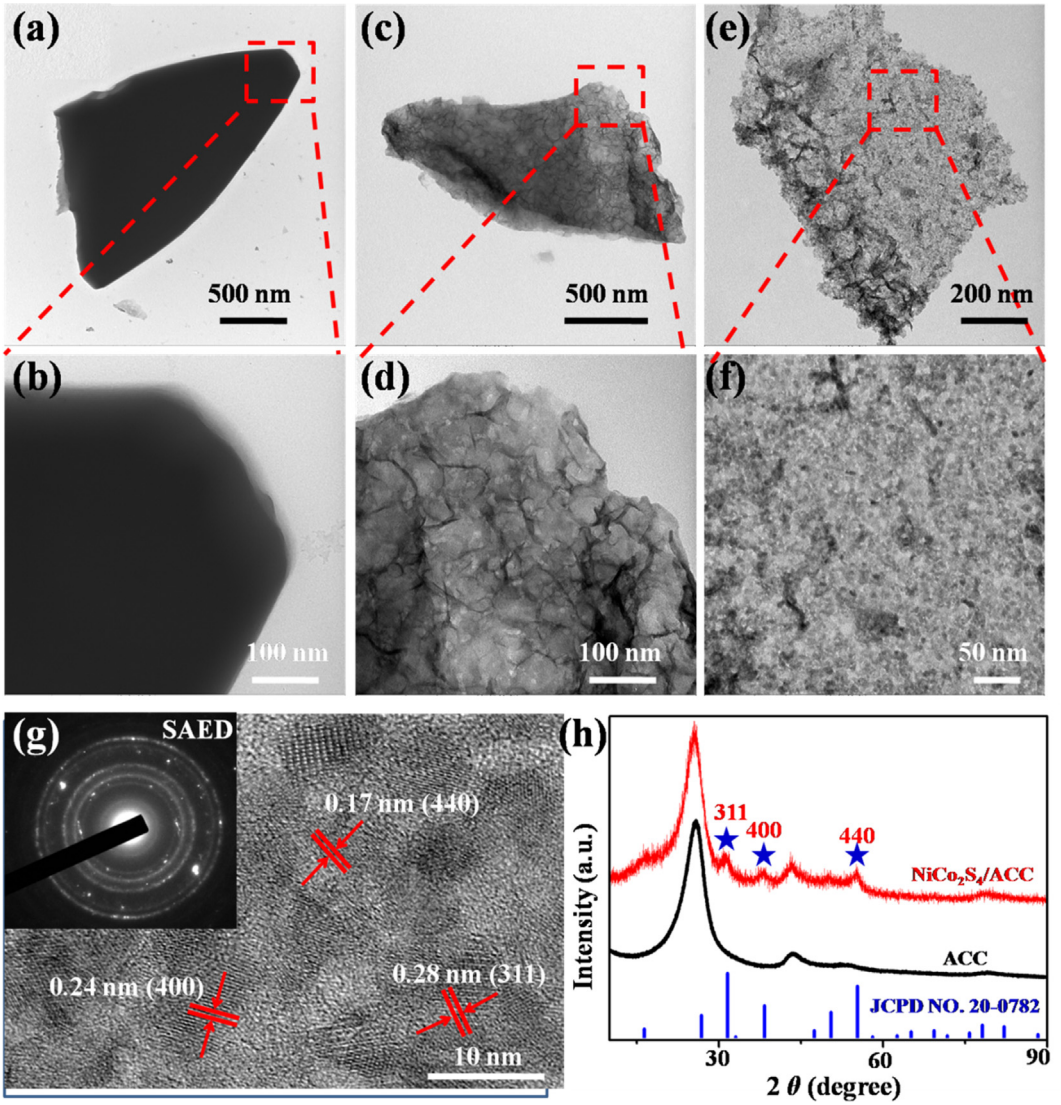

Fig. 2. TEM images of Co-MOF/ACC (a, b), Co-Ni LDH (c, d) and Ni-Co-S/ACC-160 (e, f). (g, h) HRTEM and XRD of Ni-Co-S/ACC-160, inset represents the corresponding SAED patterns.

series resistance (Rs) of Ni-Co-S/ACC-160 is 0.9 O, which is smaller than those of Ni-Co-S/ACC-120 (1.1 O) and Ni-Co-S/ACC-200 (1.0 O) respectively. The lowest Rw, Rct and Rs should contribute to the integrated ultrathin and hollow structure of the nanosheets obtained at sulfuration temperature of 160 °C, which could facilitate the ion diffusion and fast charge transfer during the redox reaction. Besides, reaction at relatively low hydrothermal temperature of 120 °C led to inferior crystallinity (Fig. S5) of the Ni-Co-S nanosheets (Fig. S6a-b) while at a much higher temperature of 200 °C the nanoparticles assembled nanosheets of generated product (Fig. S6c-e) were easy to collapse due to the excessive fast ion exchange reaction between OH^- and S^{2-}. In a word, the two products obtained at 120 °C and 200 °C failed to facilitate the ion diffusion and provide sufficient redox acting sites.

Fig. 4d shows the CV curves of Ni-Co-S/ACC-160 at different scan rates ranging from 5 to 50 mV/s. It can be observed that the oxidation peaks shift to positive potentials while the reduction peaks shift to negative potentials as the scan rates increase. This can be associated with the increment of internal diffusion resistance, which limits the ion diffusion to satisfy the electronic neutralization during the fast faradic reaction [30–32]. The CV curves could still keep a pair of well-defined redox peaks at a high scan rate of 50 mV/s, manifesting the good rate property. Moreover, a good linear relationship between the reduction or oxidation peak current density and square root of scan rate can be derived as shown in Fig. S7, suggesting the redox reactions of Ni-Co-S/ACC-160 in KOH electrolyte was mainly dominated by OH^- diffusion rate controlled process [33].

GCD curves of Ni-Co-S/ACC-160 at various current densities from 1 to 20 A/g exhibit excellent symmetry as shown in Fig. 4e, suggesting the favorable coulombic efficiency and remarkable electrochemical capacitive performance as a result of the highly reversible Faradic redox reactions during the charge–discharge process. Based on the GCD curves in Fig. 4e and Fig. S8, the specific capacitances of Ni-Co-S/ACC-120, Ni-Co-S/ACC-160 and Ni-Co-S/ACC-200 at current density of 1 A/g were calculated to be 1774, 2392 and 1424 F/g, respectively. The relationship between specific capacitance and current density is presented in Fig. 4f, from which we can see the better rate performance of Ni-Co-S/ACC-120 and Ni-Co-S/ACC-160 which are 82.5% and 80.3% at 20 A/g, respectively, while the rate performance of Ni-Co-S/ACC-200 is only 64.6% at the same current density. Cycling performance is a vital parameter when assessing the electrode materials for the practical applications of supercapacitors.

The cycling stability of Ni-Co-S-160/ACC was evaluated by GCD tests at a high current density of 30 A/g and 85.1% of the initial capacitance was retained after 10,000 cycles as shown in Fig. 4g. It is

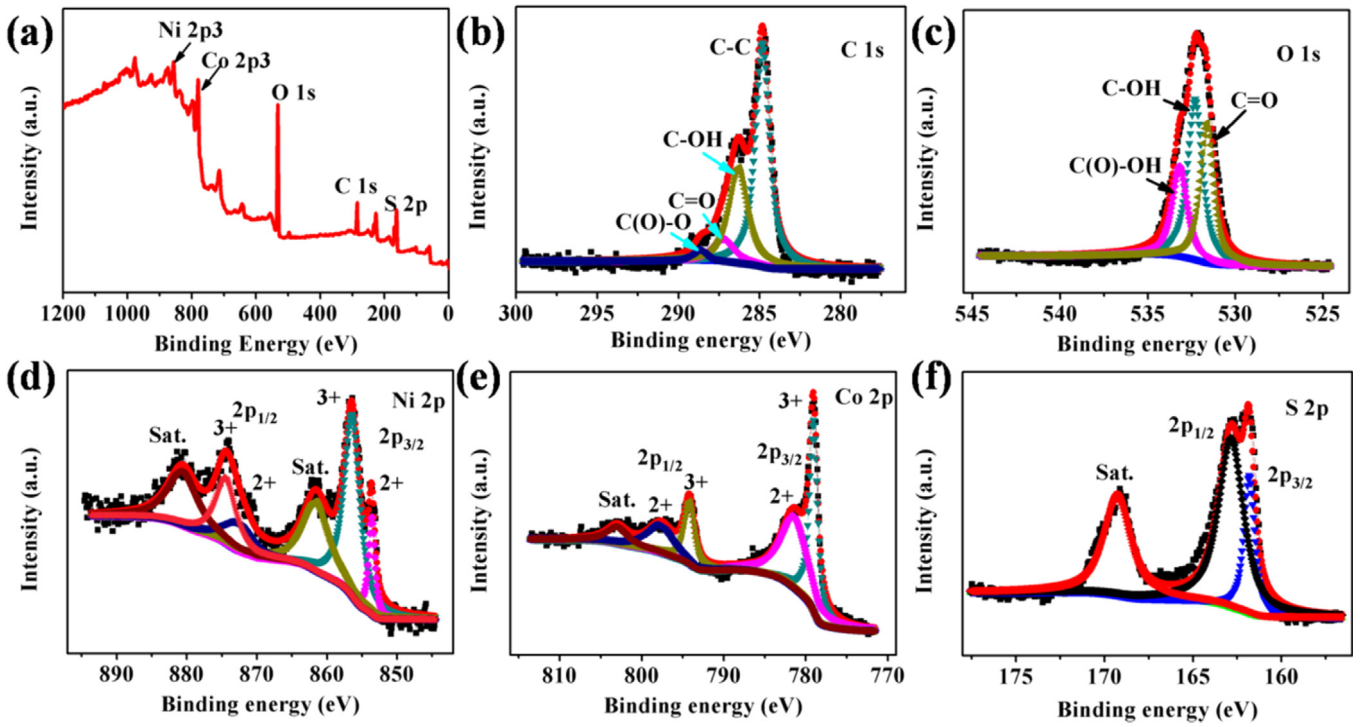

Fig. 3. XPS spectra of Ni-Co-S/ACC-160. The survey spectrum (a) and high-resolution of XPS spectra for C 1s (b), O 1s (c), Ni 2p (d), Co 2p (e) and S 2p (f), respectively.

worth noting that within 2000 cycles after the start of the test, the performance decreased slightly due to the surface of electrode not being wetted sufficiently and the lower utilization factor of electroactive materials [32,34]. As cycling numbers increased, the wettability and utilization of the electroactive materials were increased, resulting in the gradual enhancement of capacitance between 2000 and 4000 cycles [35]. After 4000 cycles, the performance decay became quite slow and ended up with a satisfactory capacity retention of 85.1% even after 10,000 cycling test, indicating the long lifespan and excellent durability. The inset was the corresponding SEM image after cycling test, from which we can observe the morphology of Ni-Co-S/ACC-160 nanoarrays was well maintained without obvious aggregation or destruction. The structural stability should result in the good electrochemical long term stability.

The excellent specific capacitance, rate performance and cycling stability should be attributed to comprehensive factors as illustrated in Fig. 4h: Firstly, as binder-free current collector the electrochemical activated carbon cloth with superb hydrophilic property has two remarkable roles: the first one is to facilitate the growth of $NiCo_2S_4$ nanosheets and the second one is to favor the penetration of electrolyte for charge storage and delivery. Secondly, the porous and hollow structure of the MOF derived ultrathin $NiCo_2S_4$ nanosheets provides more active sites and fast charge transfer path from nanosheets to carbon fiber, which are beneficial to the high-rate performance. Furthermore, $NiCo_2S_4$ nanosheets on ACC have a mixed composition containing Ni^{2+}, Ni^{3+}, Co^{2+} and Co^{3+}, which have the high electrochemical performance for supercapacitors by providing rich Faradic reactions:[36]

$$NiCo_2S_4 + OH^- + H_2O \leftrightarrow NiS_{4-4x}OH + 2CoS_{2x}OH + e^-$$

$$CoS_{2x}OH + OH^- \leftrightarrow CoS_{2x}O + H_2O + e^-$$

$$CoS_{2x}O + OH^- \leftrightarrow CoS_{2x}OH + e^-$$

$$NiS_{4-4x} + OH^- \leftrightarrow NiS_{4-4x}OH + e^-$$

Although the Ni-Co-S/ACC-160electrode has delivered a high specific performance, the relatively narrow operated potential window (0–0.55 V) will be a bottleneck when it is utilized for the energy device. Hence, the activated carbon on electrochemical activated carbon cloth (AC/ACC) was utilized as negative electrode to broaden the operated potential window and the Ni-Co-S/ACC-160 as the positive electrode with a polyvinyl alcohol (PVA)-KOH gel electrolyte as illustrated in Fig. 5a when assembling an all-solid-state asymmetric hybrid supercapacitor. The electrochemical performance of AC/ACC electrode was evaluated in a three-electrode system with 6 M KOH solution as electrolyte. The similar rectangular CV curves and symmetric linear charge–discharge curves of negative electrode AC/ACC (Fig. S9) display the fast ions diffusion/adsorption process controlled double layer capacitor behavior. AC/ACC delivers a high specific capacitance of 177 F/g at 1 A/g and maintains 94 F/g even at high current density of 20 A/g. Fig. 5b shows that the working potential ranges of Ni-Co-S-160/ACC and AC/ACC electrode at 20 mV/s are −1 to 0 V and 0–0.55 V, respectively. The mass loading of positive and negative electrodes was calculated by the following equation according to the charge balance relationship:

$$\frac{m_+}{m_-} = \frac{C_-\Delta E_-}{C_+\Delta E_+}$$

where m (g) is the mass loading of electrodes, C (F/g) represents the specific capacitance and ΔE (V) represents the charge-discharge potential window.

Fig. 5c displays CV curves of the as-synthesized ASC at different operating voltage windows, from which we can see the stable voltage could be broadened up to 1.6 V at the constant scan rate of 20 mV/s. The CV curves of ASC were acquired at the scan rates ranging from 5 to 50 mV/s as shown in Fig. 5d, demonstrating the integrated contribution of electric double-layer capacitance and battery-type capacitance with the stable operating voltage window of 0–1.6 V. Markedly, the redox peaks could still be observed from CV curve even at 50 mV/s, which indicates a good rate capacity and reaction kinetics. The symmetric GCD curves without obvious IR drop in Fig. 5e could be utilized to calculate the specific capacitance which ranged from 83.2 to 47.5F/g when the current density increased from 1 to 10 A/g, manifesting a fine coulombic efficiency and electrochemical reversibility as displayed in

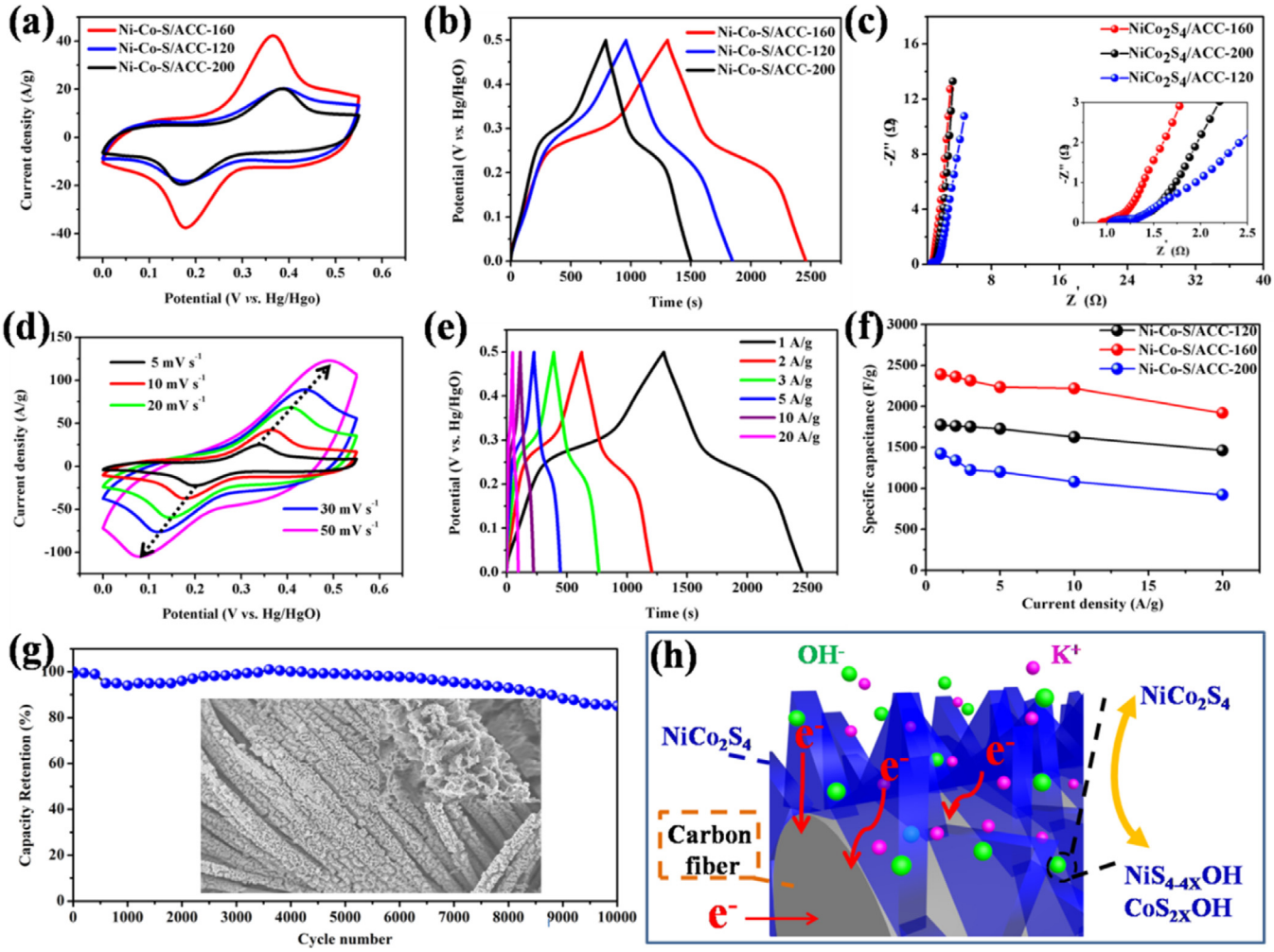

Fig. 4. (a) Cyclic voltammetry (CV) curves of Ni-Co-S/ACC-120, Ni-Co-S/ACC-160 and Ni-Co-S/ACC-200 at a scan rate of 10 mV/s. (b) Galvanostatic charge discharge (GCD) curves at 1 A/g and (c) Nyquist plots for all the Ni-Co-S electrodes. (d) CV curves at different scan rates and (e) GCD curves at different current densities of Ni-Co-S/ACC-160. (f) Specific capacitances calculate from GCD curves of all the Ni-Co-S electrodes, respectively. (g) Cycling performance of Ni-Co-S/ACC-160 at current density of 30 A/g. (h) Schematic illustration for the mechanism of charging and discharging processes for Ni-Co-S/ACC-160 electrode.

Fig. S10. Fig. 5f shows the cycling stability of ASC at the current density of 5 A/g and 82% of capacitance was retained after 10,000 cycles.

As shown in Fig. 6a the Ragone plots exhibit the high energy density of 30.1 Wh/kg at the power density of 800.2 W/kg, which still maintains 16.89 Wh/kg at a high power density of 7800 W/kg. These values are comparable or superior to those of cobalt–nickel based supercapacitors previously reported [26,37–43]. To further investigate the potential of assembled ASC in the application of portable and flexible wearable devices, a series of characterizations were performed to investigate its mechanical flexibility and electrochemical durability. As presented in Fig. 6b, the CV curves obtained after bending the ASC at 60°, 90° and 180° under the scan rate of 15 mV/s are almost overlapped, revealing the excellent flexibility and stability. As the maximum working voltage can reach to 1.6 V, three assembled hybrid supercapacitors were connected and utilized to illumine power a LED bulb. Fig. 6c displays a series of digital photos taken at different time, from which it can be seen that the LED bulb could be lighted up for more than 90 s. Furthermore, we also showed the application of hybrid supercapacitors as a wristband to power an electronic watch for more than 8 min as presented in Fig. 6d, further demonstrating the excellent flexibility and wearability with stable electrochemical performance.

4. Conclusion

In summary, we have successfully prepared hollow and ultrathin nickel cobalt sulfides nanosheets arrays on electrochemical activated carbon cloth (Ni-Co-S/ACC), where the Ni-Co-S nanosheets are derived from the metal-organic framework via an etching/ion exchange method. The $NiCo_2S_4$/ACC-160 electrode material demonstrates the high specific capacitance of 2392 F/g at the current density of 1 A/g and an outstanding capacitance retention of 80.3% under ultimate charge/discharge condition (1920 F/g at 20 A/g). A flexible hybrid supercapacitor is also successfully assembled and exhibits a high energy density of 30.1 Wh/Kg at the power density of 800.2 W/Kg and excellent electrochemical stability with capacitance ratio achieves 82% after 10,000 cycles. Impressively, the flexible hybrid supercapacitor can light up a LED bulb when three of it are connected in series. The flexible hybrid supercapacitor can also be utilized to fabricate a wristband supercapacitor that can charge a watch. Therefore, the assembled $NiCo_2S_4$/ACC device could envision great potential in other portable and wearable energy storage devices.

Acknowledgments

This work was supported by Qingdao Innovation Leading Expert Program, Taishan Scholars Program, National Natural Science

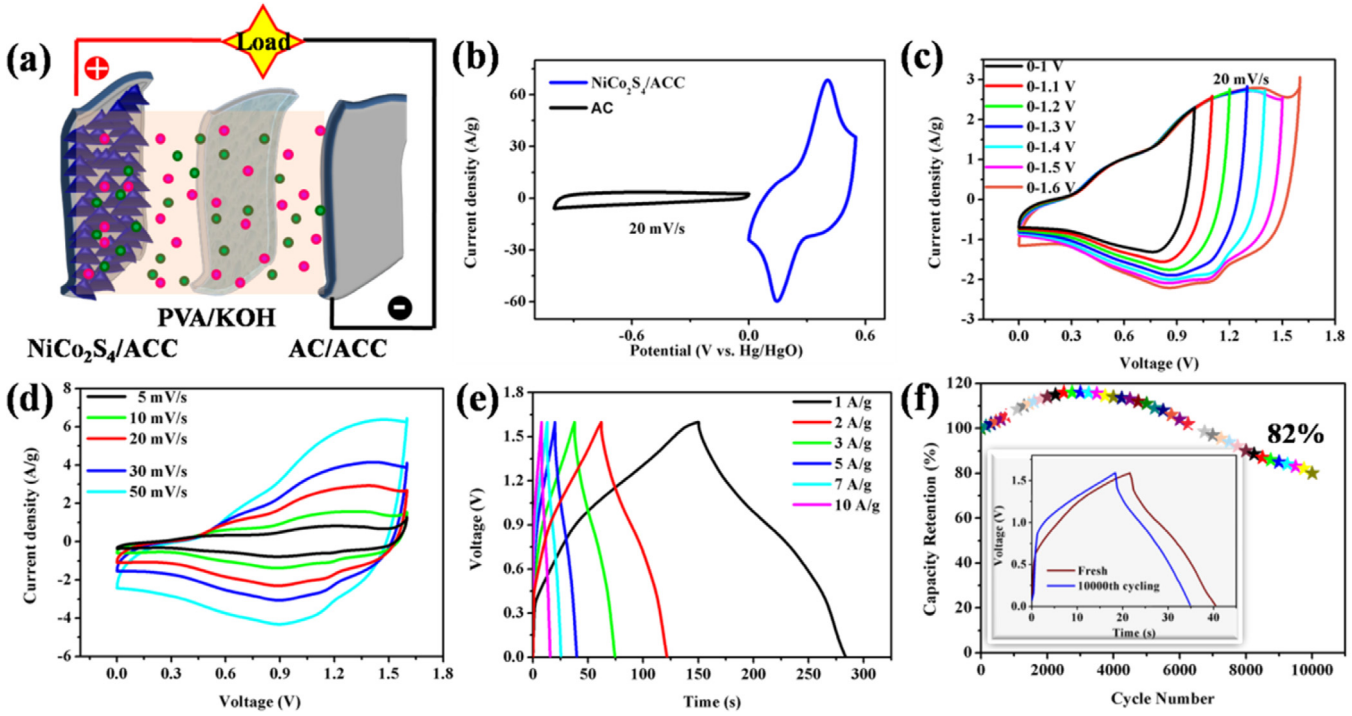

Fig. 5. (a) Schematic diagram of the assembled hybrid supercapacitor device. (b) CV curves of the positive Ni-Co-S/ACC-160 electrode and negative AC/ACC electrode at the scan rate of 20 mV/s. (c) CV curves of ASC collected at various potential windows at a scan rate of 20 mV/s and (d) at different scan rates ranging from 5 to 50 mV/s. (e) GCD curves of ASC at different current densities in the voltage range of 0 to 1.6 V. (f) Cycling performance of ASC at a scan rate of 5 mV/s, the inset represents the GCD curves before and after 10,000 cycling test.

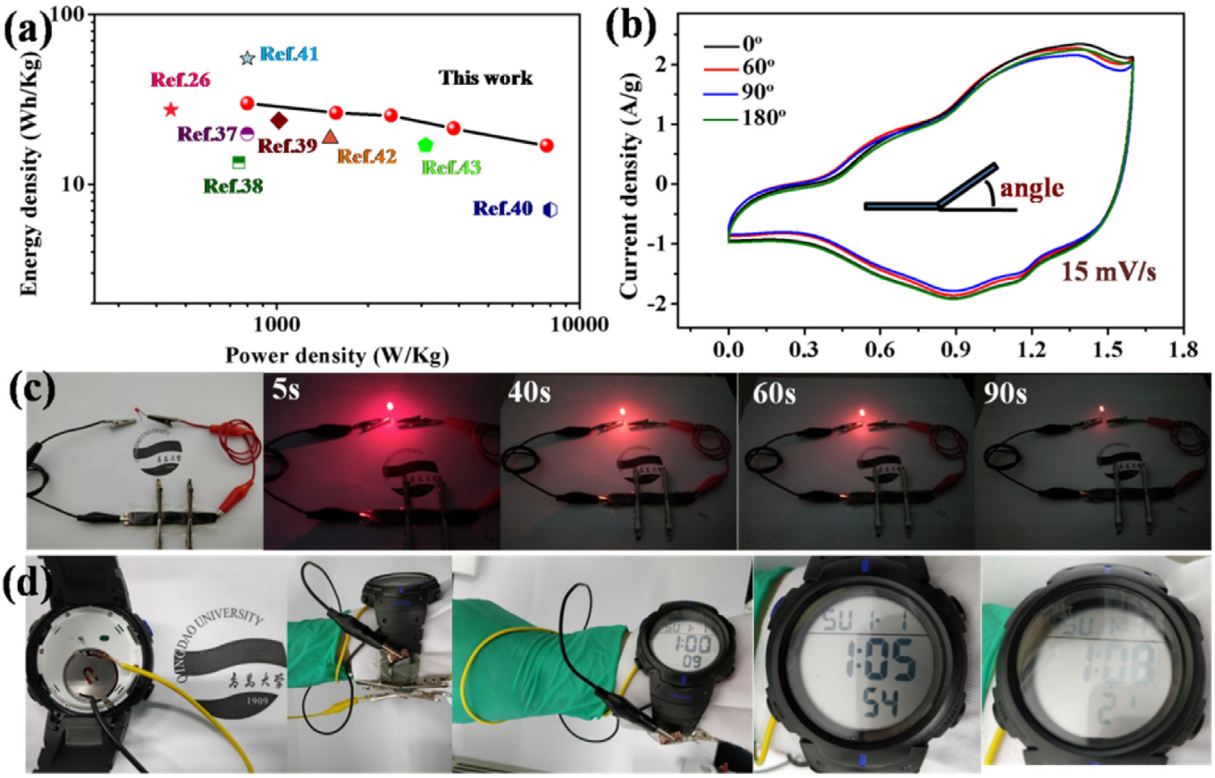

Fig. 6. (a) Comparison of energy density and power density for the assembled hybrid supercapacitor in this work with others previously reported in literatures. (b) CV curves of the prepared supercapacitor obtained with different bending angles at 15 mV/s. (c) Brightness of light-emitting diode (LED) bulb recorded at different time. (d) Application of the charged three supercapacitors as a wristband to operate an electronic watch.

Foundation of China (21805124), and Natural Science Foundation of Shandong Province (ZR2018BEM020).

Appendix A. Supplementary data

Supplementary data to this article can be found online at https://doi.org/10.1016/j.cej.2019.04.070.

References

[1] J. Tang, M. Jin, Y. Ping, Y. Fu, X. Ma, Large-area, Ultrathin inorganic network coverages–graphene hierarchical electrodes for flexible, heat-resistant energy storage application, Adv. Energy Mater. 6 (2016) 1600146.

[2] P. Geng, S. Zheng, T. Hao, R. Zhu, Z. Li, C. Shuai, H. Xue, H. Pang, Transition metal sulfides based on graphene for electrochemical energy storage, Adv. Energy Mater. 15 (2018) 1703259.

[3] L. Wang, X. Jiao, P. Liu, Y. Ouyang, X. Xia, W. Lei, Q. Hao, Self-template synthesis of yolk-shelled $NiCo_2O_4$ spheres for enhanced hybrid supercapacitors, Appl. Surf. Sci. 427 (2017) 174–181.

[4] L. Li, Z. Wu, S. Yuan, X.B. Zhang, Advances and challenges for flexible energy storage and conversion devices and systems, Energ. Environ. Sci. 7 (2014) 2101–2122.

[5] Y. Yang, R. Gedeng, X. Changsheng, W. Gunuk, J.M. Tour, Flexible three-dimensional nanoporous metal-based energy devices, J. Am. Chem. Soc. 136 (2014) 6187–6190.

[6] Y. Wang, Y. Song, Y. Xia, Electrochemical capacitors: mechanism, materials, systems, characterization and applications, Chem. Soc. Rev. 45 (2016) 5925–5950.

[7] L. Hua, Z. Hui, Y. Sun, X. Zhao, W. Huang, Oxygen vacancy enriched hollow cobaltosic oxide frames with ultrathin walls for efficient energy storage and biosensing, Nanoscale 10 (2018) 21006–21012.

[8] P. Shi, R. Chen, L. Li, J. An, L. Hua, J. Zhou, B. Liu, P. Chen, W. Huang, G. Sun, Holey nickel hydroxide nanosheets for wearable solid-state fiber-supercapacitors, Nanoscale 10 (2018) 5442–5448.

[9] K. Rui, X. Wang, M. Du, Y. Zhang, Q. Wang, Z. Ma, Q. Zhang, D. Li, X. Huang, G. Sun, Dual-function metal-organic frameworks based wearable fibers for gas probing and energy storage, ACS Appl. Mater. Interfaces 10 (2017) 2837–2842.

[10] Q. Qian, Q. Hu, L. Li, P. Shi, J. Zhou, J. Kong, X. Zhang, G. Sun, W. Huang, Sensitive fiber microelectrode made of nickel hydroxide nanosheets embedded in highly-aligned carbon nanotube scaffold for nonenzymatic glucose determination, Sensor. Actuat. B-Chem. 257 (2018) 23–28.

[11] P. Shi, R. Chen, L. Hua, L. Li, Y. Gong, C. Yu, J. Zhou, B. Liu, G. Sun, Highly concentrated, ultrathin nickel hydroxide nanosheet ink for wearable energy storage devices, Adv. Mater. 29 (2017) 1703455.

[12] H. Tong, W.L. Bai, S. Yue, Z. Gao, L. Lu, L. Shen, S. Dong, J. Zhu, J. He, X. Zhang, Zinc cobalt sulfide nanosheets grown on nitrogen-doped graphene/carbon nanotube film as high-performance electrode for supercapacitors, J. Mater. Chem. A 4 (2016) 11256–11263.

[13] J. Xiao, L. Wan, S. Yang, F. Xiao, S. Wang, Design hierarchical electrodes with highly conductive $NiCo_2S_4$ nanotube arrays grown on carbon fiber paper for high-performance pseudocapacitors, Nano Lett. 14 (2014) 831–838.

[14] T.-Y. Wei, C.-H. Chen, H.-C. Chien, S.-Y. Lu, C.-C. Hu, A cost-effective supercapacitor material of ultrahigh specific capacitances: spinel nickel cobaltite aerogels from an epoxide-driven sol-gel process, Adv. Mater. 22 (2010) 347–351.

[15] Y. Zhao, X. He, R. Chen, Q. Liu, J. Liu, J. Yu, J. Li, H. Zhang, H. Dong, M. Zhang, A flexible all-solid-state asymmetric supercapacitors based on hierarchical carbon cloth@$CoMoO_4$@NiCo layered double hydroxide core-shell heterostructures, Chem. Eng. J. 352 (2018) 29–38.

[16] W. Li, M. Tu, R. Cao, R.A. Fischer, Metal-organic framework thin films: Electrochemical fabrication techniques and corresponding applications & perspectives, J. Mater. Chem. A 4 (2016) 12356–12369.

[17] D. Sheberla, J.C. Bachman, J.S. Elias, C.J. Sun, Y. Shao-Horn, M. Dincäf, Conductive MOF electrodes for stable supercapacitors with high areal capacitance, Nat. Mater. 16 (2017) 220–224.

[18] L. Wang, X. Feng, L. Ren, Q. Piao, J. Zhong, Y. Wang, H. Li, Y. Chen, B. Wang, Flexible solid-state supercapacitor based on a metal-organic framework interwoven by electrochemically-deposited PANI, J. Am. Chem. Soc. 137 (2015) 4920–4923.

[19] W. Chen, C. Xia, H.N. Alshareef, One-step electrodeposited nickel cobalt sulfide nanosheet arrays for high-performance asymmetric supercapacitors, ACS Nano 8 (2014) 9531–9541.

[20] T. Xu, G. Li, L. Zhao, Ni-Co-S/$Co(OH)_2$ nanocomposite for high energy density all-solid-state asymmetric supercapacitors, Chem. Eng. J. 336 (2018) 602–611.

[21] J. Luo, X. Xia, Y. Luo, C. Guan, J. Liu, X. Qi, C.F. Ng, T. Yu, H. Zhang, H.J. Fan, Rationally designed hierarchical TiO_2@Fe_2O_3 hollow nanostructures for improved lithium ion storage, Adv. Energy Mater. 3 (2013) 737–743.

[22] W. Hu, R. Chen, W. Xie, L. Zou, N. Qin, D. Bao, $CoNi_2S_4$ nanosheet arrays supported on nickel foams with ultrahigh capacitance for aqueous asymmetric supercapacitor applications, ACS Appl. Mater. Interfaces 6 (2014) 19318–19326.

[23] J. Zhao, H. Lai, Z. Lyu, Y. Jiang, K. Xie, X. Wang, Q. Wu, L. Yang, Z. Jin, Y. Ma, Hydrophilic hierarchical nitrogen-doped carbon nanocages for ultrahigh supercapacitive performance, Adv. Mater. 27 (2015) 3541–3545.

[24] K. Xiao, L.X. Ding, G. Liu, H. Chen, S. Wang, H. Wang, Freestanding, hydrophilic nitrogen-doped carbon foams for highly compressible all solid-state supercapacitors, Adv. Mater. 28 (2016) 5997–6002.

[25] J. Huang, J. Wei, Y. Xiao, Y. Xu, Y. Wang, L. Tan, K. Yuan, Y. Chen, When Al-doped cobalt sulfide nanosheets meet nickel nanotube arrays: a highly efficient and stable cathode for asymmetric supercapacitors, ACS Nano (2018) 3030–3041.

[26] Y. Zheng, X. Wang, W. Zhao, X. Cao, J. Liu, Phytic acid-assisted synthesis of ultrafine $NiCo_2S_4$ nanoparticles immobilized on reduced graphene oxide as high-performance electrode for hybrid supercapacitors, Chem. Eng. J. 333 (2017) 603–612.

[27] Y. Ouyang, X. Xia, H. Ye, L. Wang, X. Jiao, W. Lei, Q. Hao, Three-dimensional hierarchical structure ZnO@C@NiO on carbon cloth for asymmetric supercapacitor with enhanced cycle stability, ACS Appl. Mater. Interfaces 10 (2018) 3549–3561.

[28] C. Yuan, J. Li, L. Hou, L. Yang, L. Shen, X. Zhang, Facile template-free synthesis of ultralayered mesoporous nickel cobaltite nanowires towards high-performance electrochemical capacitors, J. Mater. Chem. 22 (2012) 16084–16090.

[29] F. Cai, G. Zhang, J. Chen, X. Gou, H. Liu, S. Dou, $Ni(OH)_2$ tubes with mesoscale dimensions as positive-electrode materials of alkaline rechargeable batteries, Angewandte Chemie(German Edition) 116 (2004) 4308–4312.

[30] C. Zhang, J. Xiao, X. Lv, L. Qian, S. Yuan, S. Wang, P. Lei, Hierarchically porous Co_3O_4/C nanowire arrays derived from a metal-organic framework for high performance supercapacitors and the oxygen evolution reaction, J. Mater. Chem. A 4 (2016) 16516–16523.

[31] Y. Huang, M. Zhong, M. Zhu, Z. Pei, Z. Wang, Q. Xue, X. Xie, C. Zhi, A self-healable and highly stretchable supercapacitor based on a dual crosslinked polyelectrolyte, Nat. Commun. 6 (2015) 10310.

[32] J. Liu, M. Hu, J. Wang, N. Nie, Y. Wang, Y. Wang, J. Zhang, Y. Huang, An intrinsically 400% stretchable and 50% compressible NiCo//Zn battery, Nano Energy 58 (2019) 338–346.

[33] B.K. Lesel, J.S. Ko, B. Dunn, S.H. Tolbert, Mesoporous $LixMn_2O_4$ thin film cathodes for lithium ion pseudocapacitors, ACS Nano 10 (2016) 7572–7581.

[34] D. Zha, H. Sun, Y. Fu, X. Ouyang, W. Xin, Acetate anion-intercalated nickel-cobalt layered double hydroxide nanosheets supported on Ni foam for high-performance supercapacitors with excellent long-term cycling stability, Electrochim. Acta 236 (2017) 18–27.

[35] R. Li, S. Wang, Z. Huang, F. Lu, T. He, $NiCo_2S_4$@$Co(OH)_2$ core-shell nanotube arrays in situ grown on Ni foam for high performances asymmetric supercapacitors, J. Power Sources 312 (2016) 156–164.

[36] C. Wei, Y. Huang, S. Xue, X. Zhang, X. Chen, J. Yan, W. Yao, One-step hydrothermal synthesis of flaky attached hollow-sphere structure $NiCo_2S_4$ for electrochemical capacitor application, Chem. Eng. J. 317 (2017) 873–881.

[37] C.S. Dai, P.Y. Chien, J.Y. Lin, S.W. Chou, W.K. Wu, P.H. Li, K.Y. Wu, T.W. Lin, Hierarchically structured Ni_3S_2/carbon nanotube composites as high performance cathode materials for asymmetric supercapacitors, ACS Appl. Mater. Interfaces 5 (2013) 12168–12174.

[38] Q. Gao, X. Wang, Z. Shi, Z. Ye, W. Wang, N. Zhang, Z. Hong, M. Zhi, Synthesis of porous $NiCo_2S_4$ aerogel for supercapacitor electrode and oxygen evolution reaction electrocatalyst, Chem. Eng. J. 331 (2017) 185–193.

[39] Y.-Y. Chen, P. Dhaiveegan, M. Michalska, J.-Y. Lin, Morphology-controlled synthesis of nanosphere-like $NiCo_2S_4$ as cathode materials for high-rate asymmetric supercapacitors, Electrochim. Acta 274 (2018) 208–216.

[40] S.G. Mohamed, I. Hussain, J.-J. Shim, One-step synthesis of hollow C-$NiCo_2S_4$ nanostructures for high-performance supercapacitor electrodes, Nanoscale 10 (2018) 6620–6628.

[41] W. He, Z. Liang, K. Ji, Q. Sun, T. Zhai, X. Xu, Hierarchical Ni-Co-S@Ni-W-O core-shell nanosheet arrays on nickel foam for high-performance asymmetric supercapacitors, Nano Res. 11 (2018) 1415–1425.

[42] H. Wang, M. Liang, D. Duan, W. Shi, Y. Song, Z. Sun, Rose-like Ni_3S_4 as battery-type electrode for hybrid supercapacitor with excellent charge storage performance, Chem. Eng. J. 350 (2018) 523–533.

[43] P. Yang, Z. Wu, Y. Jiang, Z. Pan, W. Tian, L. Jiang, L. Hu, Fractal $(NixCo_{1-x})_9Se_8$ nanodendrite arrays with highly exposed (011) surface for wearable, all-solid-state supercapacitor, Adv. Energy Mater. 8 (2018) 1801392.